Bubble Simulation Using Level Set-Boundary Element Method

Tan Kiok Lim, Khoo Boo Cheong, and Jacob White

***Abstract*— In bubble dynamics, an underwater bubble may evolve from being singly-connected to being toroidal. Furthermore, two or more individual bubbles may merge to form a single large bubble. These dynamics involve significant topological changes such as merging and breaking, which may not be handled well by front-tracking boundary element methods. In the level set method, topological changes are handled naturally through a higher-dimensional level set function. This makes it an attractive method for bubble simulation.**

In this paper, we present a method that combines the level set method and the boundary element method for the simulation of bubble dynamics. We propose a formulation for the update of a potential function in the level set context. This potential function is non-physical off the bubble surface but consistent with the physics on the bubble surface. We consider only axisymmetric cavitation bubbles in this paper. Included in the paper are some preliminary results and findings.

I. Introduction

THE dynamics of underwater bubbles has been a subject of interest for some time. Interesting observations include, when a bubble is initiated close to a rigid boundary, the formation of a jet directed towards the rigid boundary [1], and when a bubble is initiated close to the free surface, the formation of a jet directed away from the free surface [2][3]. There are more complex phenomena, such as a bubble becoming doubly-connected [4] and multiple bubbles combining. An established method for such simulations is based on an Eulerian-Lagrangian formulation which combines the front-tracking method and the boundary element method ([1][2][3], for example). The implementation of this method becomes more complicated as bubbles merge or become doubly-connected, in particular for simulations in 3D [5].

The level set method [6][7], which embeds the physical interface in a higher-dimensional function, provides a natural way of handling complex topological changes. The level set method has been used in the simulation of bubbles ([8][9], for example), together with the incompressible Navier-Stokes equation.

We know of only two published works which combine the level set method and boundary integral formulation. Sethian and Strain [10] used this method to model crystal growth. Li and Cai [11] used the method to simulate dynamic powder consolidation of metals. In [11], the unknown on the boundary is computed based on given boundary conditions. In [10], the unknown which the boundary integral equation is used to compute, is off the boundary. A separate function defining a physical quantity on and off the boundary also serves as input to the boundary integral equation.

In this paper, we develop a level set-boundary element formulation for the simulation of an *axisymmetric cavitation* bubble based on potential flow. This formulation differs from [11] in that a separate potential function is evolved together with the level set function. The potential function, defined in the level set context, is evolved with the condition that the potential on the zero level set is consistent with Bernoulli's equation. This then serves as the boundary condition to the boundary integral equation from which the unknown, the normal velocity of the bubble surface, is computed. Just as with the level set function, this potential function has no physical meaning off the zero level set. This, together with the fact that the unknown is on the boundary itself, differentiates our formulation from that in [10].

In Section II, we present the mathematical formulation and proposed update equation for the potential function. We give an outline of the algorithm in Section III and details of the numerical implementation in Section IV. Some preliminary results are discussed in Section V before we conclude in Section VI.

Since the level set method and front-tracking method considered here both utilise the boundary element method, we shall henceforth drop the "boundary element" from our references to the two methods.

II. Mathematical Formulation

A. Velocity Potential and Boundary Integral Formulation

A schematic diagram of the problem is given in Fig. 1. Assuming incompressibility and irrotationality, the liquid is then governed by Laplace's equation

$$\nabla^2 \phi = 0$$

with the liquid velocity given by

$$\vec{v} = \nabla \phi$$

where ϕ is the velocity potential. The above may then be formulated as a boundary integral problem governed by

$$c(p)\,\phi(p) + \int_S \phi(q)\,\frac{\partial}{\partial n}\left(\frac{1}{|p-q|}\right) dS = \int_S \frac{\partial \phi(q)}{\partial n}\,\frac{1}{|p-q|}\,dS \qquad (1)$$

Tan Kiok Lim is a Ph.D. student at the Singpore-MIT Alliance (SMA), Singapore (e-mail: smap9055@nus.edu.sg).

Khoo Boo Cheong is an Associate Professor with the Department of Mechanical Engineering, National University of Singapore, Singapore, and an SMA Fellow.

Jacob White is a Professor with the Department of Electrical Engineering and Computer Science, Massachusetts Institute of Technology (MIT), Cambridge, Massachusetts, USA, and an SMA Fellow.

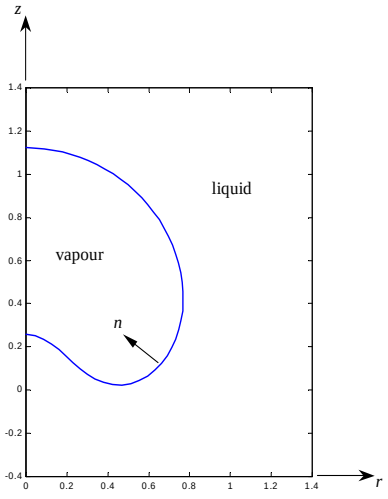

Fig. 1. Schematic Diagram of Problem.

where p is a load point, q is a field point, S denotes the bubble surface and n is the direction normal to S away from the liquid (Fig. 1). We refer the reader to [13] and [14] for details on the axisymmetric boundary integral formulation for potential problems.

The dynamic boundary condition on the bubble surface is governed by the unsteady Bernoulli's equation [15]

$$\frac{\partial \phi}{\partial t} = 1 - \frac{1}{2}\left|\nabla\phi\right|^2 - \delta^2\left(z-\gamma\right) \tag{2}$$

where t denotes time, δ is the buoyancy parameter, z is the depth (Fig. 1) and γ is the inception depth of the bubble. All the values in (2) has been non-dimensionalised.

B. Level Set Method

The level set method represents a physical interface implicitly as the zero level set in a higher-dimensional level set function [6][7]. The update equation for the level set function is given by

$$\frac{\partial \psi}{\partial t} + F\left|\nabla\psi\right| = 0 \tag{3}$$

where ψ is the level set function and F is the normal velocity function. In this paper, the zero level set represents the bubble surface.

C. Bernoulli's Equation

The *Eulerian* form of the unsteady Bernoulli's equation is given by (2). The *Lagrangian* form is given by ([3], for example)

$$\begin{aligned}\frac{d\phi}{dt} &= \frac{\partial\phi}{\partial t} + \nabla\phi\cdot\nabla\phi \\ &= 1 + \frac{1}{2}\left|\nabla\phi\right|^2 - \delta^2\left(z-\gamma\right).\end{aligned} \tag{4}$$

The above update equation is based on the surface moving with its material velocity. Alternatively, if the update equation is based on the surface moving with its normal velocity, the equation would then be

$$\begin{aligned}\frac{d_n\phi}{dt} &= \frac{\partial\phi}{\partial t} + \left(v_n\,\underline{\vec{n}}\right)\cdot\nabla\phi \\ &= 1 - \frac{1}{2}\left|\nabla\phi\right|^2 - \delta^2\left(z-\gamma\right) + v_n^2\end{aligned} \tag{5}$$

where $\frac{d_n}{dt}$ represents the time derivative following the surface moving with its normal velocity, $v_n = \nabla\phi\cdot\underline{\vec{n}}$ and $\underline{\vec{n}}$ is the unit normal to the surface. We highlight that ϕ, z and v_n are values pertaining to the bubble surface.

D. Proposed Potential Function and Update Equation

Let $\tilde{\phi}$ be the potential function defined in the level set context. As with the level set function, we set $\tilde{\phi}$ to be a higher-dimensional function with the condition

$$\tilde{\phi}\left(x_S\right) = \phi\left(x_S\right) \tag{6}$$

where x_S is any point that satisfies $\psi\left(x_S\right) = 0$ and ϕ is the velocity potential on the bubble surface consistent with Bernoulli's equation.

Since the level set function is propagated using the normal velocity, we base our proposed formulation on (5). The aim is to construct an update equation which maintains (6). The proposed potential update equation is given by

$$\frac{\partial\tilde{\phi}}{\partial t} + F\left(\nabla\tilde{\phi}\cdot\frac{\nabla\psi}{\left|\nabla\psi\right|}\right) = 1 - \frac{1}{2}V^2 - \delta^2\left(Z-\gamma\right) + F^2 \tag{7}$$

where F, V and Z are extension values such that

$$F \to v_n,\ V \to \left|\nabla\phi\right|,\ Z \to z \quad \text{as} \quad \psi \to 0. \tag{8}$$

As stated in [12] for F, there is much flexibility in the choice of F, V and Z. Here, we construct extension values of the form

$$\begin{aligned}\nabla F\cdot\nabla\psi &= 0 \\ \nabla V\cdot\nabla\psi &= 0 \\ \nabla Z\cdot\nabla\psi &= 0\end{aligned}$$

as given in [12]. A proof of consistency of the proposed equation is given as follows. Because of (8), (7) may be written as

$$\frac{\partial\tilde{\phi}}{\partial t} + F\left(\nabla\tilde{\phi}\cdot\underline{\vec{n}}\right) = 1 - \frac{1}{2}\left|\nabla\phi\right|^2 - \delta^2\left(z-\gamma\right) + v_n^2 \tag{9}$$

on the bubble surface since $\frac{\nabla\psi}{\left|\nabla\psi\right|} = \underline{\vec{n}}$ at $\psi = 0$. If $\tilde{\phi}$ in (9) is replaced by the true velocity potential ϕ, (9) will then be identical to (5), which concludes the proof.

III. Outline of Numerical Algorithm

An outline of the proposed level set algorithm is given as follows. At time-step k, assume ψ^k and $\tilde{\phi}^k$ are known. Perform:

1) Interpolate ψ^k and $\tilde{\phi}^k$ to obtain the position of the bubble surface and ϕ^k, the potential on the bubble surface respectively. Please refer to Section IV.B. for details.
2) Based on the position of the bubble surface and ϕ^k, compute the normal velocity v_n^k and the tangential velocity v_t^k of the bubble surface using (1) and a cubic spline fit respectively. Please refer to Section IV.C. for details.
3) Compute $\left|\nabla\phi^k\right| = \sqrt{\left(v_n^k\right)^2 + \left(v_t^k\right)^2}$, the magnitude of material velocity of the bubble surface.
4) Extend v_n^k, $\left|\nabla\phi^k\right|$ and z^k to all grid points to obtain F^k, V^k and Z^k respectively. Please refer to Section IV.D. for details.
5) Compute ψ^{k+1} and $\tilde{\phi}^{k+1}$ using (3) and (7) respectively. Please refer to Section IV.E. for details.
6) Set $t^{k+1} = t^k + \Delta t$.

For the initial conditions, we specify a spherical bubble of radius R^0 centered at $(0, \gamma)$ with a constant potential ϕ^0. From these, we generate ψ^0 and $\tilde{\phi}^0$, both being signed distance functions, to begin the computation.

IV. Details of Numerical Implementation

The numerical implementation details are given below. For clarity, the superscript k denoting the time-step has been omitted.

A. Grid Discretisation

There are essentially two grids, a moving grid for the boundary element method and a fixed grid for the level set method. A schematic diagram of the two grids at a particular time-step is given in Fig. 2. The boundary element grid is represented by the solid line with dots and changes at every time-step, following the position of the bubble surface. The discretisation procedure for the boundary element method is given in Section IV.C. The fixed level set grid is represented by the dotted lines. The computational domain is $0 \leq r \leq 1.2$ and $-1.0 \leq z \leq 1.4$ with grid size $h = \Delta r = \Delta z$.

B. Establishing the Position of and Potential on the Bubble Surface

In order to establish the position of the bubble surface, we find the points where $\psi = 0$ intersects the grid. We follow the method given in [10] except that we make use of cubic interpolation instead of linear interpolation. This is done by approximating ψ along the grid line by a third-order Newton's divided difference equation and computing the position of the root using Newton's method. We refer to these points as *intersection points*. Let n^{int} denote the number of intersection points, and r^{int} and z^{int} denote the position of the set of intersection points found.

Having obtained the position of the intersection points, the potential at these points is computed using a third-order Newton's divided difference approximation of $\tilde{\phi}$ along the same grid line. Let ϕ^{int} denote these potential values.

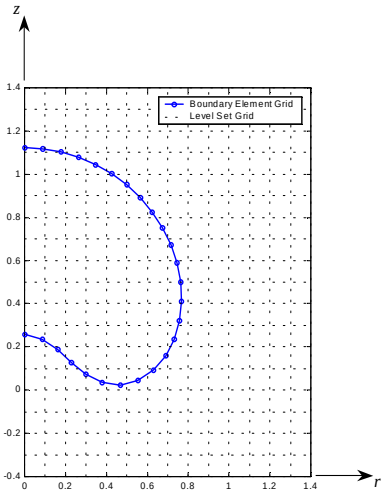

Fig. 2. Schematic Diagram of Boundary Element Grid and Level Set Grid.

C. Computation of the Normal Velocity and Tangential Velocity

The computation of normal velocity involves the discretisation of (1). Here, we follow the method given in [16] except for the representation of the bubble surface and the computation of the tangential velocity. In [16], the bubble surface is represented using linear elements. In this paper, we use a cubic spline representation of the bubble surface. The procedure for computing the normal velocity is given as follows.

1) From r^{int} and z^{int}, compute the segment length between each pair of intersection points based on the Euclidean distance. Let ξ be the arc length parameter along the bubble surface. Compute the value of ξ for each intersection point by summing the individual segment lengths.
2) Use cubic splines [17] to interpolate r^{int}, z^{int} and ϕ^{int}. Compute the position and potential at n^{knot} equidistant points along ξ. We refer to these equidistant points as *knots* and let the computed position and potential be denoted by r^{knot} and z^{knot}, and ϕ^{knot} respectively.
3) Discretise (1) based on r^{knot}, z^{knot} and ϕ^{knot} using, except for the representation of the bubble surface, the method given in [16]. Here, we make use of the cubic splines obtained previously with r^{int} and z^{int} to compute $r, z, \frac{\partial r}{\partial \xi}$ and $\frac{\partial z}{\partial \xi}$ at each quadrature point. Compute the normal velocity at the knots v_n^{knot}.
4) Use a cubic spline to interpolate v_n^{knot}. The normal velocity $v_n(\xi)$ at any point on the bubble surface may then be obtained.
5) From the cubic spline that interpolates ϕ^{int}, the tangential velocity $v_t(\xi)$ at any point on the bubble surface may be obtained.

D. Extension Values

We compute the extension values F, V and Z on all grid points by extending v_n, $|\nabla\phi|$ and z respectively from the appropriate points on the bubble surface. This is done using the higher-order method given in [18]. In this paper, we use a second-order scheme.

E. Update Equations

We discretise (3) using the entropy-satisfying upwind scheme given in [6]. We use a third-order ENO scheme to obtain the spatial derivatives and a third-order Runge-Kutta TVD scheme for the time-stepping [19]. We make use of the same discretisation scheme for (7).

V. Preliminary Results and Discussion

In the test case, we use $h = 0.05$, $n^{knot} = 26$, $\delta^2 = 0.25$, $\gamma = 0.0$, $R^0 = 0.6$ and $\phi^0 = -0.9333$ with the level set code. We compare the results from the test case to the results obtained from the established front-tracking method based on (4) using identical parameters. We further compare the results from the test case to the results obtained from the front-tracking method based on (5) using the same parameters.

The spatial discretisation of the front-tracking method used for comparison follows that of [16] while the time discretisation follows that of [3]. For the spatial discretisation, we make use of 51 points (50 segments) to define the bubble surface. For the time discretisation, we use $\Delta\phi = 0.02$ with the front-tracking code based on (4) to compute the time-step size Δt. We make use of the same Δt in our level set code and the front-tracking code based on (5) to facilitate comparison.

A comparison of the results from the level set code (represented by solid lines) to the results from the front-tracking code based on (4) (represented by dots) is given in Figs. 3 through 10. The comparison of position of the bubble surface at $t = 0.0, 0.689, 1.296$ and 1.494 is given in Figs. 3, 5, 7 and 9 respectively while the comparison of potential, normal velocity and tangential velocity along the bubble surface is given in Figs. 4, 6, 8 and 10 respectively.

Figs. 11 through 18 compare the results from the level set code (represented by solid lines) to the results from the front-tracking code based on (5) (represented by triangles). The comparison of position of the bubble surface at $t = 0.0, 0.689, 1.296$ and 1.494 is given in Figs. 11, 13, 15 and 17 respectively while the comparison of potential, normal velocity and tangential velocity along the bubble surface is given in Figs. 12, 14, 16 and 18 respectively.

Since the front-tracking method based on (4) is well established, we base our discussion on the comparison made against this method. It is observed in Fig. 4 that there is a difference in the normal velocities at $t = 0.0$. Because of the higher-order representation of surface used, the normal velocity computed by the level set code is, in fact, more accurate than the normal velocity computed by the front-tracking code. This can be verified against the analytic solution. It is also observed in Fig. 4 that the tangential velocity from the level set code is oscillatory. However, we note that the magnitude of these oscillations are of $\mathrm{O}\,(1\mathrm{e}-13)$.

In Figs. 5 through 8, the results from the two codes correspond well to each other. Although the computed position of the bubble surface from the two codes correspond well to each other at $t = 1.494$ (Fig. 9), some oscillations are observed in the normal and tangential velocities computed using the level set code (Fig. 10).

From the results above, we observe that our present algorithm works well during the initial and intermediate stages of bubble evolution. Some instabilities begin to appear as the simulation progresses to an advanced stage of evolution.

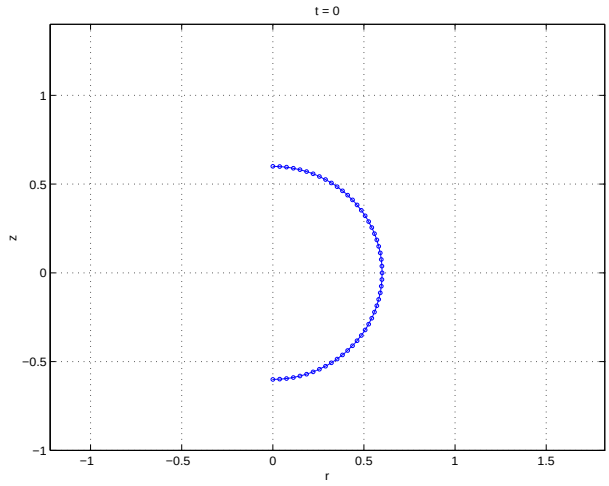

Fig. 3. Comparison of Position of Bubble Surface at $t = 0.0$. Front-Tracking Method Based on (4).

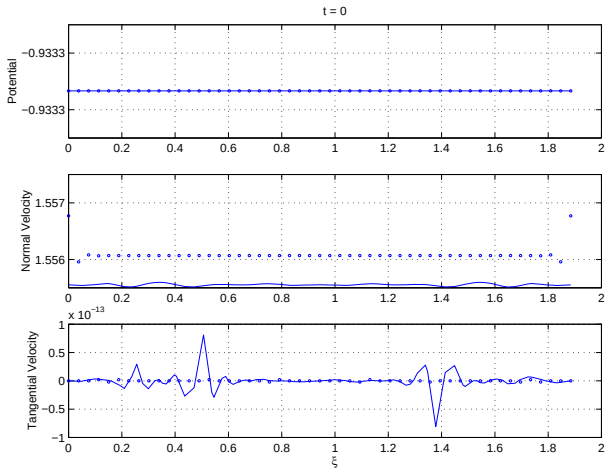

Fig. 4. Comparison of Potential, Normal Velocity and Tangential Velocity at $t = 0.0$. Front-Tracking Method Based on (4).

VI. Conclusion

In this paper, we have presented an algorithm that combines the level set method and boundary element method for the simulation of axisymmetric cavitation bubbles based on potential flow. This includes a potential function in the level set context together with an update equation that maintains consistency of potential on the bubble surface. The use of this method allows topological changes to be handled naturally, thereby facilitating the simulation of complex bubble dynamics. We have shown in our results that the algorithm works well during the initial and intermediate stages of evolution. Our future work will be focused on eliminating the instabilities observed, thus ensuring simulation of the bubble into the advanced stages of evolution.

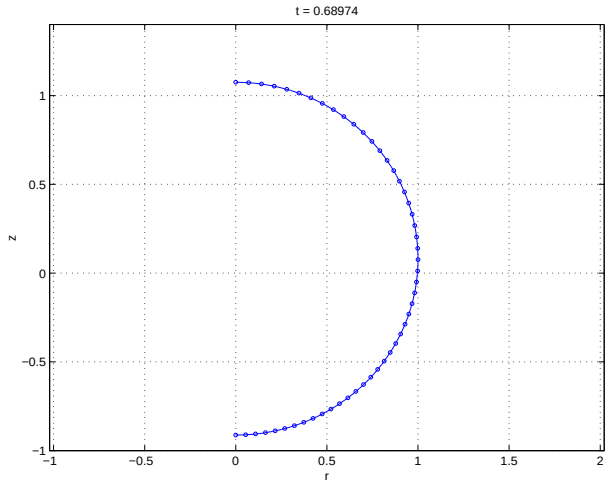

Fig. 5. Comparison of Position of Bubble Surface at $t = 0.689$. Front-Tracking Method Based on (4).

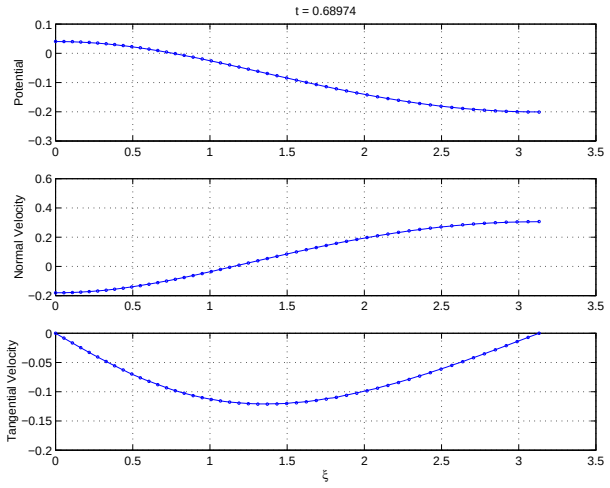

Fig. 6. Comparison of Position of Bubble Surface at $t = 0.689$. Front-Tracking Method Based on (4).

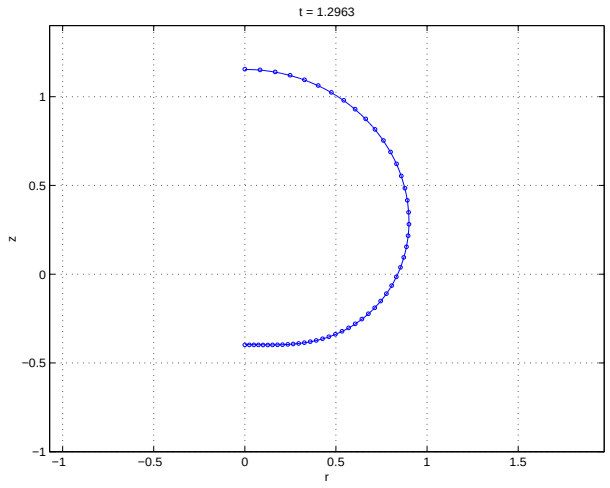

Fig. 7. Comparison of Position of Bubble Surface at $t = 1.296$. Front-Tracking Method Based on (4).

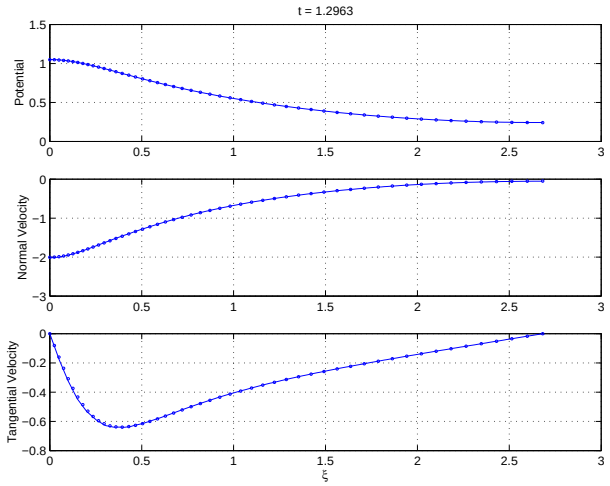

Fig. 8. Comparison of Potential, Normal Velocity and Tangential Velocity at $t = 1.296$. Front-Tracking Method Based on (4).

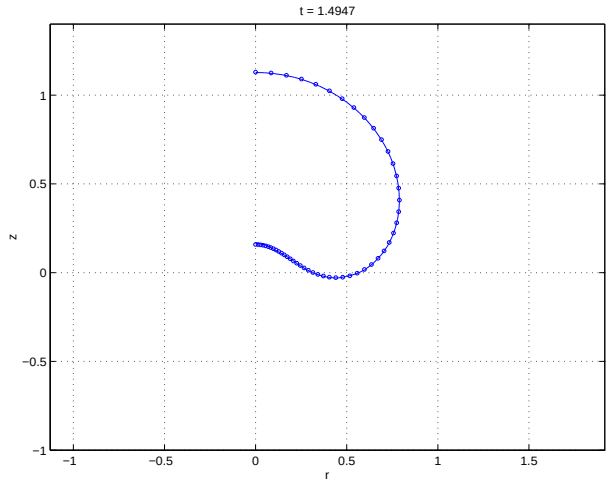

Fig. 9. Comparison of Position of Bubble Surface at $t = 1.494$. Front-Tracking Method Based on (4).

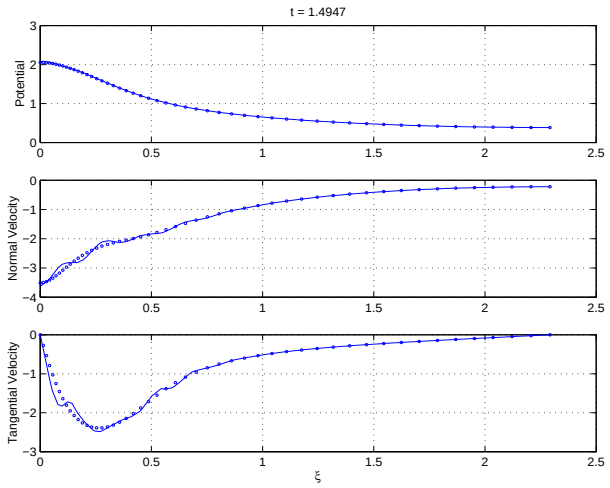

Fig. 10. Comparison of Potential, Normal Velocity and Tangential Velocity at $t = 1.494$. Front-Tracking Method Based on (4).

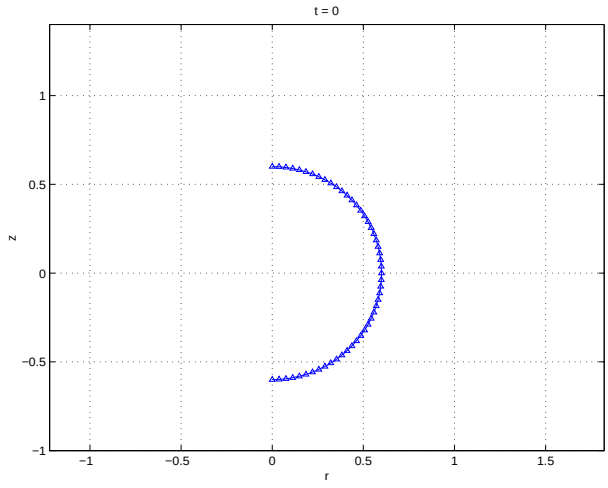

Fig. 11. Comparison of Position of Bubble Surface at $t = 0.0$. Front-Tracking Method Based on (5).

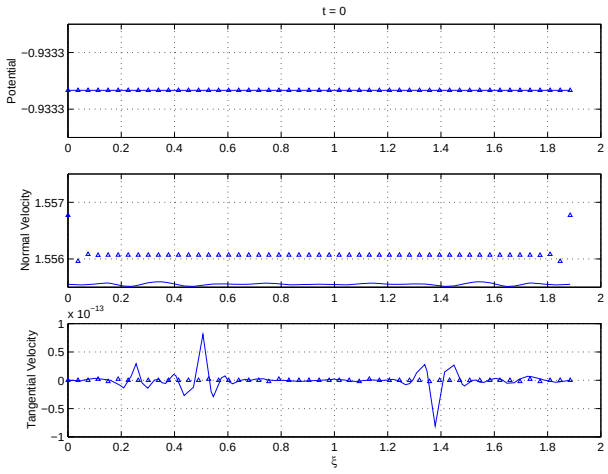

Fig. 12. Comparison of Potential, Normal Velocity and Tangential Velocity at $t = 0.0$. Front-Tracking Method Based on (5).

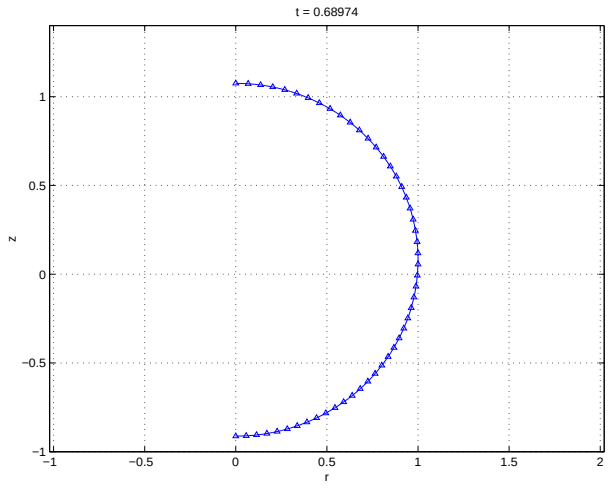

Fig. 13. Comparison of Position of Bubble Surface at $t = 0.689$. Front-Tracking Method Based on (5).

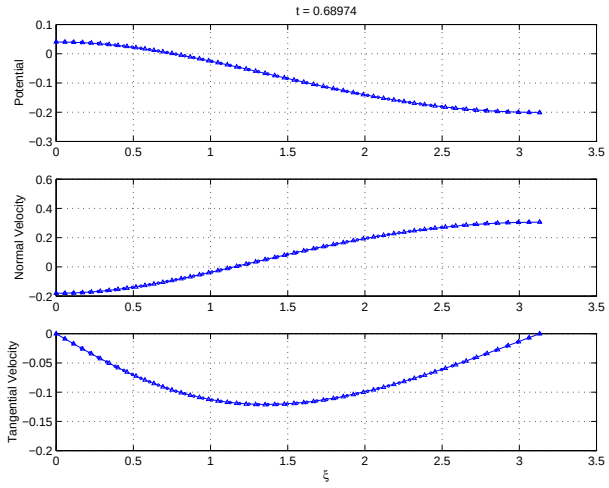

Fig. 14. Comparison of Position of Bubble Surface at $t = 0.689$. Front-Tracking Method Based on (5).

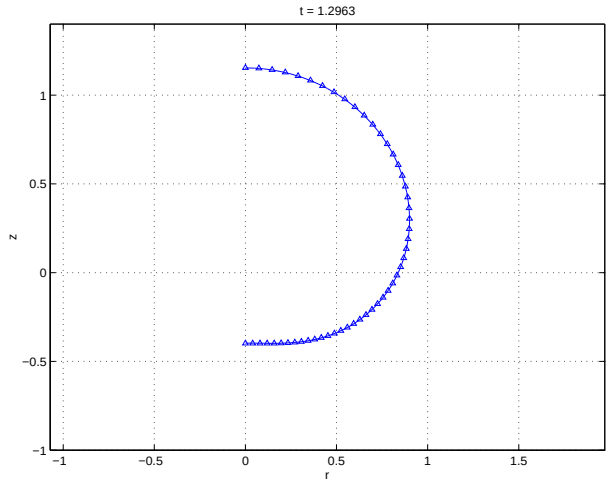

Fig. 15. Comparison of Position of Bubble Surface at $t = 1.296$. Front-Tracking Method Based on (5).

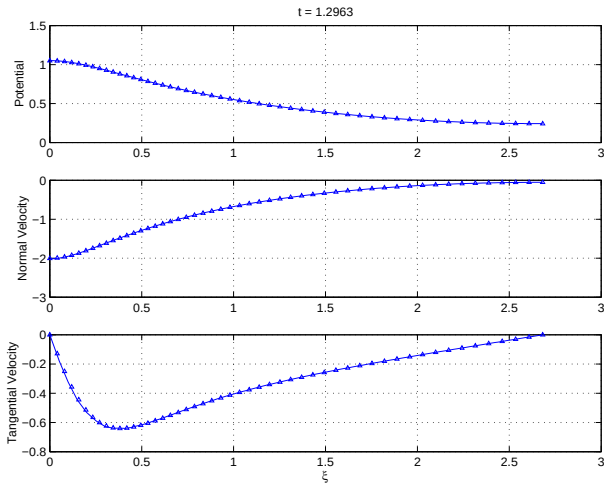

Fig. 16. Comparison of Potential, Normal Velocity and Tangential Velocity at $t = 1.296$. Front-Tracking Method Based on (5).

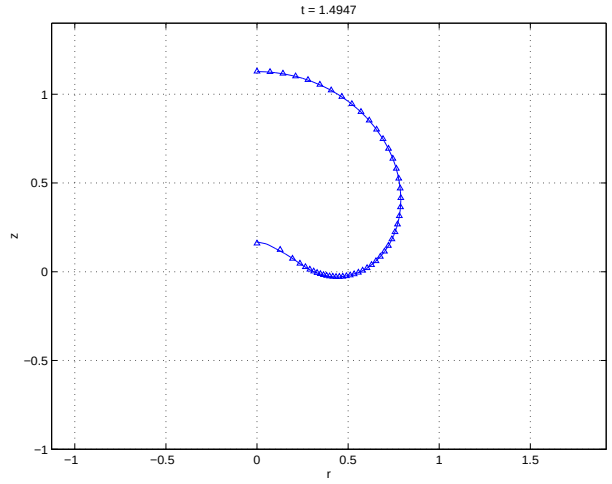

Fig. 17. Comparison of Position of Bubble Surface at $t = 1.494$. Front-Tracking Method Based on (5).

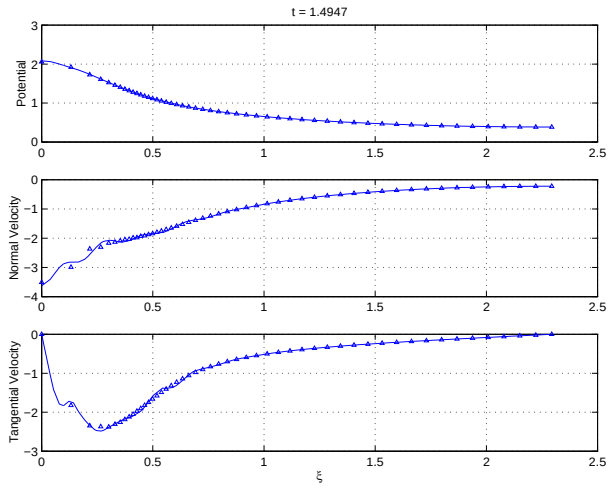

Fig. 18. Comparison of Potential, Normal Velocity and Tangential Velocity at $t = 1.494$. Front-Tracking Method Based on (5).

ACKNOWLEDGMENTS

The authors would like to thank Prof. J. Peraire of MIT, and Dr. E. Klaseboer, Dr. T. G. Liu and Dr. C. Wang of the Institute of High Performance Computing for their many helpful discussions.

REFERENCES

[1] J. R. Blake, B. B. Taib, and G. Doherty, "Transient Cavities Near Boundaries. Part 1. Rigid Boundary," *Journal of Fluid Mechanics*, Vol. 170, pp. 479–497, 1986.

[2] J. R. Blake, B. B. Taib, and G. Doherty, "Transient Cavities Near Boundaries. Part 2. Free Surface," *Journal of Fluid Mechanics*, Vol. 181, pp. 197–212, 1987.

[3] Q. X. Wang, K. S. Yeo, B. C. Khoo, and K. Y. Lam, "Strong Interaction Between a Buoyancy Bubble and a Free Surface," *Theoretical and Computational Fluid Dynamics*, Vol. 8, pp. 73–88, 1996.

[4] Q. X. Wang, K. S. Yeo, B. C. Khoo, and K. Y. Lam, "Nonlinear Interaction Between Gas Bubble and Free Surface," *Computers & Fluids*, Vol. 25, pp. 607–628, 1996.

[5] Y. L. Zhang, K. S. Yeo, B. C. Khoo, and C. Wang, "3D Jet Impact and Toroidal Bubbles," *Journal of Computational Physics*, Vol. 166, pp. 336–360, 2001.

[6] J. A. Sethian, "Evolution, Implementation, and Application of Level Set and Fast Marching Methods for Advancing Fronts," *Journal of Computational Physics*, Vol. 169, pp. 503–555, 2001.

[7] S. Osher, and R. P. Fedkiw, "Level Set Methods: An Overview and Some Recent Results," *Journal of Computational Physics*, Vol. 169, pp. 463–502, 2001.

[8] M. Sussman, E. Fatemi, P. Smereka, and S. Osher, "An Improved Level Set Method for Incompressible Two-Phase Flows," *Computers & Fluids*, Vol. 27, pp. 663–680, 1998.

[9] Y. C. Chang, T. Y. Hou, B. Merriman, and S. Osher, "A Level Set Formulation of Eulerian Interface Capturing Methods for Incompressible Fluid Flows," *Journal of Computational Physics*, Vol. 124, pp. 449–464, 1996.

[10] J. A. Sethian, and J. Strain, "Crystal Growth and Dendritic Solidification," *Journal of Computational Physics*, Vol. 98, pp. 231–253, 1992.

[11] Z. Li, and W. Cai, "A Level Set-Boundary Element Method for Simulation of Dynamic Powder Consolidation of Metals," in *Numerical Analysis and Its Applications 2000, Lecture Notes in Computer Science 1988*, (eds. L. Vulkov, J. Waśniewski, and P. Yalamov), pp. 527–534, Springer-Verlag, 2001.

[12] D. Adalsteinsson, and J. A. Sethian, "The Fast Construction of Extension Velocities in Level Set Methods," *Journal of Computational Physics*, Vol. 148, pp. 2–22, 1999.

[13] A. A. Becker, *The Boundary Element Method in Engineering. A Complete Course*. McGraw-Hill Book Company, 1992.

[14] A. A. Bakr, *The Boundary Integral Equation Method in Axisymmetric Stress Analysis Problems*. Springer-Verlag, 1986.

[15] J. R. Blake, J. M. Boulton-Stone, and R. P. Tong, "Boundary Integral Methods for Rising, Bursting and Collapsing Bubbles," in *BE Applications in Fluid Mechanics*, (ed. H. Power), pp. 31–72, Computational Mechanics Publications, 1995.

[16] B. B. Taib, *Boundary Integral Method Applied to Cavitation Bubble Dynamics*. Ph.D. thesis, University of Wollongong, 1985.

[17] W. H. Press, S. A. Teukolsky, W. T. Vetterling, and B. P. Flannery, *Numerical Recipes in FORTRAN. The Art of Scientific Computing. Second Edition*. Cambridge University Press, 1992.

[18] D. L. Chopp, "Some Improvements of the Fast Marching Method," *SIAM Journal on Scientific Computing*, Vol. 23, pp. 230–244, 2001.

[19] S. Osher, and C.-W. Shu "High-Order Essentially Nonoscillatory Schemes for Hamilton-Jacobi Equations," *SIAM Journal on Numerical Analysis*, Vol. 28, pp. 907–922, 1991.